

CARL: A Framework for Equivariant Image Registration

Hastings Greer

University of North Carolina at Chapel Hill

Lin Tian

University of North Carolina at Chapel Hill

François-Xavier Vialard
Université Gustave Eiffel

Roland Kwitt
University of Salzburg

Raul San Jose Estepar
Harvard Medical School

Marc Niethammer
University of North Carolina at Chapel Hill

Abstract

Image registration estimates spatial correspondences between a pair of images. These estimates are typically obtained via numerical optimization or regression by a deep network. A desirable property of such estimators is that a correspondence estimate (e.g., the true oracle correspondence) for an image pair is maintained under deformations of the input images. Formally, the estimator should be equivariant to a desired class of image transformations. In this work, we present careful analyses of the desired equivariance properties in the context of multi-step deep registration networks. Based on these analyses we 1) introduce the notions of $[U, U]$ equivariance (network equivariance to the *same* deformations of the input images) and $[W, U]$ equivariance (where input images can undergo *different* deformations); we 2) show that in a suitable multi-step registration setup it is sufficient for overall $[W, U]$ equivariance if the first step has $[W, U]$ equivariance and all others have $[U, U]$ equivariance; we 3) show that common displacement-predicting networks only exhibit $[U, U]$ equivariance to translations instead of the more powerful $[W, U]$ equivariance; and we 4) show how to achieve multi-step $[W, U]$ equivariance via a coordinate-attention mechanism combined with displacement-predicting refinement layers (CARL). Overall, our approach obtains excellent practical registration performance on several 3D medical image registration tasks and outperforms existing unsupervised approaches for the challenging problem of abdomen registration.

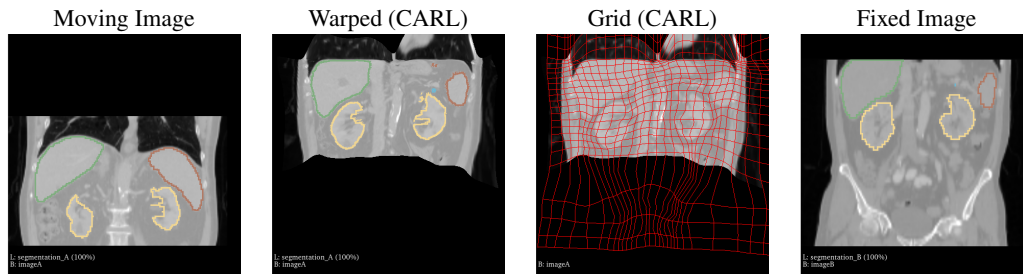


Figure 1: Example image registration result on a pair from the Abdomen1k dataset. We particularly highlight that CARL’s equivariance helps it to tackle very large displacements and differing fields of view.

1 Introduction

Image registration is an important task in medical image computing [41]. There is extensive research into solving this problem with deep learning [47, 3, 29, 39]. In particular, unsupervised deep learning methods [13, 45] have attained strong performance on many benchmarks [20]. We present an equivariant registration layer that can be inserted into an unsupervised multi-step registration network, which makes the overall registration architecture equivariant to independently translated images.

Notation. We denote the moving and fixed images as I^M and I^F , respectively. They are functions $\Omega \rightarrow \mathbb{R}^D$, where Ω is the image domain, and D is typically 1 for a single channel imaging modality. Further, we denote a registration algorithm as a capital Greek letter, such as Φ . In our notation, a registration algorithm can be applied to a pair of images by square brackets, i.e. $\Phi [I^M, I^F]$, and a registration algorithm, when thus applied to a pair of images, yields a map $\mathbb{R}^N \rightarrow \mathbb{R}^N$ (ideally a diffeomorphism) that can be post-composed with the moving image to yield a function that is close to the fixed image, i.e.,

$$I^M \circ \Phi [I^M, I^F] \sim I^F. \quad (1)$$

With this notation, we can define what it means for a registration algorithm to be *equivariant*. Conceptually, equivariance means that when the input images are warped, correspondence between the registered images is preserved; it is not required that the correspondence is *correct*, only that it is *the same* before and after applying a warp to the input images. We say a registration algorithm Φ is $[W, U]$ *equivariant* with respect to a class of transforms \mathcal{T} if correspondence is preserved when the images are warped *independently*. Formally, this means

$$\forall W, U \in \mathcal{T}, \Phi [I^M \circ W, I^F \circ U] = W^{-1} \circ \Phi [I^M, I^F] \circ U. \quad (2)$$

As a weaker form of equivariance, we say a registration algorithm is $[U, U]$ *equivariant* if correspondence is preserved when the images are warped *together*, i.e.,

$$\forall U \in \mathcal{T}, \Phi [I^M \circ U, I^F \circ U] = U^{-1} \circ \Phi [I^M, I^F] \circ U. \quad (3)$$

From our analysis (Sec. 3), it will be clear that both definitions are well justified.

2 Related work

We review related work at the intersection of equivariance (and how to achieve it) and image registration, as well as previous work on unsupervised learning of neural networks for image registration.

Equivariant encoders. The most impactful equivariant layers in the field of neural networks have been ordinary convolution [11] and attention [32], which are equivariant to translation and permutation, respectively. In this work, we focus on using attention and convolution to make a registration algorithm that is by construction $[W, U]$ equivariant to translation. However, there are also more recent approaches to create components with additional geometric equivariances such as to rotation. These include group equivariant convolution [7], StyleGAN’s equivariant convolution [23], and spherical harmonic convolution [30]. These should be explored in future work to expand the deformations with respect to which our approach (based on what we call *coordinate attention*, see Sec. 4) is $[W, U]$ equivariant.

Keypoint-based equivariant registration architectures. Several registration approaches relying on keypoint matching have been proposed [26, 4]. Notably, any approach that aligns keypoints to keypoints using a least squares fit is $[W, U]$ equivariant to rigid motions if the keypoint selectors and descriptors are equivariant to rigid motions. The reason can be derived from the notion of equivariance as follows: *if two points correspond before warping the input images, they should correspond afterwards*. The keypoints align with each other before and after a warp is applied, and move with features on the input images when they are warped. SURF [4] and related methods fall under this category in the subfield of non-learning-based 2D image alignment. For medical image registration, learning-based approaches that leverage keypoints include EasyReg [22], Keymorph [48], SAME++ [40] and E-CNN [6]. SAME++ [40] uses a pretrained foundation model as a convolutional encoder, and extracts matched keypoints from it using methods traditionally used in 2D image

feature alignment, such as checking for cycle consistency. This alignment is then refined using a trained deep network with overall strong performance on lung, abdomen, and head/neck computed tomography (CT) registration tasks. EasyReg, E-CNN and KeyMorph achieve equivariant registration by locating a fixed set of keypoints in each image and aligning matching keypoints. EasyReg’s [22] affine pre-registration is by construction $[W, U]$ equivariant to affine deformations because it works by segmenting the brain images to be registered, and then bringing the centroids of the segmented regions into alignment. In effect, this uses each segmented region as a keypoint. In our experiments (see Sec. 6) we will see that this strategy works well even for out-of-distribution translations, and exhibits strong performance when detailed segmentations are available for training. In the KeyMorph work of [45], equivariance is achieved in an unsupervised setting by learning to predict keypoints in brain images. Unlike SURF and related approaches, KeyMorph avoids the need for a matching step by predicting keypoints in a fixed order. Finally, in the E-CNN work of [6], the authors leverage a rotationally equivariant encoder built using spherical harmonics to predict features, and the centers of mass of each feature channel are then used as keypoints and rigidly aligned in a differentiable manner. The network is trained by warping a single image with two different transforms and then penalizing the difference between the network output and the transform used to generate the pair.

Equivariance losses. Several works aim for equivariance via suitably designed loss terms. In the CoMIR work of [31], for instance, the authors train an image encoder to be equivariant to rotations and deformations using an unsupervised contrastive loss with additional constraints. Furthermore, the concept of W -bipath consistency, introduced in [42], is effectively a penalty to encourage the $[W, U]$ equivariance to B-Spline transforms. In particular, [42] uses penalties to enforce that $\Phi[I^M, I^F \circ U] = \Phi[I^M, I^F] \circ U$ as well as inverse consistency, which together are sufficient conditions for $[W, U]$ equivariance. While this is undoubtedly useful for training (as it is equivariance enforced by a loss), it is not likely to hold for out-of-distribution data, unlike our approach which is *by construction* $[W, U]$ equivariant.

Unsupervised image registration. In addition to prior work on equivariance, we also build on research into unsupervised image registration. The foundational concept [3] driving this subfield is to predict deformations using a neural network. Training minimizes a similarity and a regularity loss. It is feasible to learn multiple steps of registration by simply penalizing the final similarity and regularity [35, 12, 39], even when the steps have different transform models [13, 35]. Diffeomorphisms can be guaranteed by special vector field integration layers [8], inversion layers [21] or *encouraged* by a loss, such as diffusion [3, 35], or inverse consistency [12, 39]. Accuracy can be improved by learning features, computing cost volumes from the similarity between features in the fixed and moving images, and predicting a transform based on this cost volume [29]. From this subfield we adopt most of GradICON [39]: we use their loss and regularity hyperparameters to produce approximately diffeomorphic transforms, adopt their learning rate and multi-step, multi-resolution approach, and use their U-Net architecture for the *refinement layers* of CARL. While replacing *Step 1* of their approach with our custom architecture Ξ_θ might appear as a minor modification, it has profound consequences which we will work out in Secs. 3-5.2. In short, this replacement makes the entire network $[W, U]$ equivariant with respect to translation, whereas GradICON and most of the standard convolution-based deep registration networks only provide the weaker $[U, U]$ equivariance.

3 Diffeomorphism to diffeomorphism registration

In Sec. 1, we defined equivariance for registration as preserving the correspondence between points in the images if they are warped before being registered. To nail down a mathematical definition, we investigate a specific class of images I^M and I^F where the correspondence is well defined: we let them have $[0, 1]^D$ as their domain and range, and require them to be diffeomorphisms. While this restricted problem does not correspond to a real-world medical registration task, it allows a closed form solution, yielding important insights that can be carried back to real registration problems where finding correspondences is not as easily tractable. Because I^M is *invertible*, we can make Eq. (1) an *equality* and then solve for the registration algorithm, which we denote as Ξ :

$$\begin{aligned}
 I^M \circ \Xi[I^M, I^F] &= I^F \\
 \Leftrightarrow (I^M)^{-1} \circ I^M \circ \Xi[I^M, I^F] &= (I^M)^{-1} \circ I^F \\
 \Leftrightarrow \Xi[I^M, I^F] &= (I^M)^{-1} \circ I^F.
 \end{aligned}
 \tag{4}$$

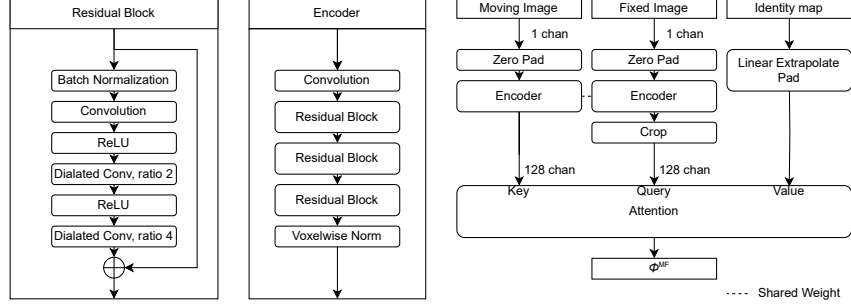


Figure 2: Architecture of Ξ_θ . The specific arrangement of pads and crops allows voxels to be mapped to points outside of Ω - this is necessary to represent translation.

Since I^M and I^F are images, and for these images Ξ is correct, a hypothetical registration algorithm that registers any pair of images correctly will output the same transforms as Ξ in situations where Ξ is valid, and hence will tend to share the equivariences of Ξ . In particular, Ξ is equivariant to the group $\text{Diff}(\mathbb{R}^N) \times \text{Diff}(\mathbb{R}^N)$ as follows. Let U and W be arbitrary members of $\text{Diff}(\mathbb{R}^N)$, then we obtain the following commutative diagram:

$$\begin{array}{ccc}
 (I^M, I^F) & \xrightarrow{x, y \mapsto x \circ W, y \circ U} & (I^M \circ W, I^F \circ U) \\
 \Xi \downarrow & & \downarrow \Xi \\
 (I^M)^{-1} \circ I^F & \xrightarrow{\varphi \mapsto W^{-1} \circ \varphi \circ U} & W^{-1} \circ (I^M)^{-1} \circ I^F \circ U
 \end{array} \tag{5}$$

Now, if we have a new registration algorithm Φ , a class of input images and potential transforms, we can check if that particular network is equivariant by checking if for all W, U the following diagram holds (if so, the registration algorithm is $[W, U]$ equivariant with respect to diffeomorphisms):

$$\begin{array}{ccc}
 (I^M, I^F) & \xrightarrow{x, y \mapsto x \circ W, y \circ U} & (I^M \circ W, I^F \circ U) \\
 \Phi \downarrow & & \downarrow \Phi \\
 \Phi[I^M, I^F] & \xrightarrow{\varphi \mapsto W^{-1} \circ \varphi \circ U} & W^{-1} \circ \Phi[I^M, I^F] \circ U
 \end{array} \tag{6}$$

In other words, if the registration algorithm results in φ for registering I^M to I^F , then it needs to be constructed such that it results in $W^{-1} \circ \varphi \circ U$ if images I^M and I^F are warped by W and U , respectively. In that case, W and U will not change the image correspondences.

In practice, we will often restrict the group from which W and U may be chosen. For example, if for a registration algorithm Φ , for any translations W and U , $\Phi[I^M \circ W, I^F \circ U] = W^{-1} \circ \Phi[I^M, I^F] \circ U$, we say that the algorithm Φ is $[W, U]$ equivariant with respect to translations.

Finally, we remark that some registration algorithms are only equivariant for applying the same transform to both images; that is, for any transform U from a group of transforms \mathcal{T} , $\Phi[I^M \circ U, I^F \circ U] = U^{-1} \circ \Phi[I^M, I^F] \circ U$. We say that such an algorithm is $[U, U]$ equivariant with respect to \mathcal{T} . This justifies the definitions we previewed in Sec. 1.

4 Coordinate attention

Our central contribution when seeking to realize $[W, U]$ equivariance is what we call *coordinate attention*, i.e., a standard attention block where the value vectors are the coordinates of each voxel. This has the effect of computing the center of mass of the attention mask associated with each query, and allows this center of mass computation to be performed using highly optimized kernels, such as flash attention [9]. As an illustrative example, in Appendix C we use coordinate attention to solve the diffeomorphism-to-diffeomorphism registration problem.

For registering medical images, we use an architecture we call Ξ_θ , a combination of coordinate attention with a feature encoder consisting of convolutional layers all operating at the same resolution,

some of which are dilated. The encoder is exactly equivariant to integer pixel translations. Edge effects are reduced by padding with zeros before running images through the feature encoder, and cropping afterwards. The architecture is illustrated in 2. It is important that the coordinate attention formulation, which is "center of mass of $\text{softmax}(QV^T)$," can be computed using a standard attention operation instead of a custom set of operations on all pairs of feature vectors. Attention has hyperoptimized implementations such as flash attention [9] that only require $\mathcal{O}(\#\text{voxels})$ memory and have excellent cache coherency. While flash attention is $\mathcal{O}(\text{image side length}^6)$, in practice performance is adequate in our setting when Ξ_θ (see Fig. 2 for the definition of Ξ_θ) is applied to a volume of size $43 \times 43 \times 43$, which is sufficient for coarse registration. We will show (in Sec. 5.2) that it is then possible to add fine grained registration while preserving $[W, U]$ equivariance.

5 Equivariance of Coordinate Attention with convolutional encoders (Ξ_θ)

We assume that the attention mask associated with each query vector has small spatial support. Finding a training procedure that reliably fulfilled this assumption across different datasets was nontrivial: we find that this assumption is valid after regularizing the network end to end with diffusion regularization for the first several epochs, and GradICON regularization thereafter.

We assume that the feature encoders are translation equivariant like

$$\text{Conv}_\theta(I \circ U) = \text{Conv}_\theta(I) \circ U. \quad (7)$$

With these assumptions, we prove that Ξ_θ is $[W, U]$ equivariant to translations as follows:

Without positional embeddings or causal masking, (we do not use either) the attention mechanism is equivariant to permutations as follows: for P_1, P_2 permutations; and the output and K (Key), Q (Query), and V (Value) inputs represented each as a function from an index to a vector, and an attention block represented as \mathbb{T} ,

$$\mathbb{T}[K \circ P_1, Q \circ P_2, V \circ P_1] = \mathbb{T}[K, Q, V] \circ P_2. \quad (8)$$

Additionally, because the attention weights in an attention block sum to 1, for an affine function f ,

$$\mathbb{T}[K, Q, f \circ V] = f \circ \mathbb{T}[K, Q, V]. \quad (9)$$

A translation W by an integer number of voxels is both affine when seen as an operation on coordinates, $W_{x \rightarrow x+r}$, and a permutation of the voxels when seen as an operation on voxel images $W_{\text{permutation}}$ – as long as we can neglect boundary effects. The map from indices to coordinates, coords, serves as the bridge between these two representations of a transform ($W_{x \rightarrow x+r} \circ \text{coords} = \text{coords} \circ W_{\text{permutation}}$). As long as the attention masks have small spatial support, we can suppress boundary effects by padding with zeros before applying the operation. So, for translations W, U , we have

$$\begin{aligned} \Xi_\theta[I^M \circ W, I^F \circ U] &:= \mathbb{T}[\text{Conv}_\theta(I^M \circ W), \text{Conv}_\theta(I^F \circ U), \text{coords}] \\ &= \mathbb{T}[\text{Conv}_\theta(I^M) \circ W, \text{Conv}_\theta(I^F) \circ U, \text{coords}] \quad \text{by (7)} \\ &= W^{-1} \circ \mathbb{T}[\text{Conv}_\theta(I^M) \circ W, \text{Conv}_\theta(I^F) \circ U, W \circ \text{coords}] \quad \text{by (9)} \\ &= W^{-1} \circ \mathbb{T}[\text{Conv}_\theta(I^M) \circ W, \text{Conv}_\theta(I^F) \circ U, \text{coords} \circ W] \\ &= W^{-1} \circ \mathbb{T}[\text{Conv}_\theta(I^M), \text{Conv}_\theta(I^F) \circ U, \text{coords}] \quad \text{by (8)} \\ &= W^{-1} \circ \mathbb{T}[\text{Conv}_\theta(I^M), \text{Conv}_\theta(I^F), \text{coords}] \circ U \quad \text{by (8)} \\ &= W^{-1} \circ \Xi_\theta[I^M, I^F] \circ U \end{aligned} \quad (10)$$

This establishes that Ξ_θ is $[W, U]$ equivariant with respect to translation.

5.1 $[U, U]$ equivariance

So far, we have pointed out that Ξ_θ is $[W, U]$ equivariant to translation. Our next goal is to show that our full approach, *Coordinate Attention with Refinement Layers* (CARL), is also $[W, U]$ equivariant to translation. To this end, we first show that VoxelMorph-like networks are $[U, U]$ equivariant to translation as they predict displacements, and then we will show that a multi-step registration

algorithm where the first step is $[W, U]$ equivariant and subsequent steps are $[U, U]$ equivariant is overall $[W, U]$ equivariant. Notably, any all-convolutional network is translationally equivariant¹:

$$\begin{array}{ccc}
 X & \xrightarrow{f \mapsto f \circ U} & \tilde{X} \\
 \text{Conv}_\theta \downarrow & & \downarrow \text{Conv}_\theta \\
 Y & \xrightarrow{f \mapsto f \circ U} & \tilde{Y}
 \end{array} \tag{11}$$

To apply a convolutional network to registration, first it is made to have two inputs by channel-wise concatenation, and it is chosen to have D output channels. Its output can then be interpreted (via interpolation) as a function from the domain of the input images to \mathbb{R}^N . If used to predict coordinates, this has a different equivariance than $[U, U]$ equivariance: to be $[U, U]$ equivariant with respect to translation, a registration algorithm needs to have a bottom arrow $f \mapsto U^{-1} \circ f \circ U$ where (11) has $f \mapsto f \circ U$. This is ameliorated in Quicksilver [47], VoxelMorph [3] and their successors by predicting displacements instead of coordinates. Overall, in VoxelMorph we have

$$\Phi_\theta[I^M, I^F](\vec{x}) := \text{Conv}_\theta[\text{cat}(I^M, I^F)](\vec{x}) + \vec{x} \ , \tag{12}$$

and by parameterizing our translation transform U by a vector \vec{r} , we can compute

$$\begin{aligned}
 \Phi_\theta[I^M \circ U, I^F \circ U](\vec{x}) &= \text{Conv}_\theta[\text{cat}(I^M \circ U, I^F \circ U)](\vec{x}) + \vec{x} \\
 &= \text{Conv}_\theta[\text{cat}(I^M, I^F) \circ U](\vec{x}) + \vec{x} = (\text{Conv}_\theta[\text{cat}(I^M, I^F)] \circ U)(\vec{x}) + \vec{x} \\
 &= \text{Conv}_\theta[\text{cat}(I^M, I^F)](U(\vec{x})) + \vec{x} = \text{Conv}_\theta[\text{cat}(I^M, I^F)](U(\vec{x})) + (\vec{x} + \vec{r}) - \vec{r} \\
 &= U^{-1} \circ (\text{Conv}_\theta[\text{cat}(I^M, I^F)](\vec{x}) + \vec{x}) \circ U = U^{-1} \circ \Phi_\theta[I^M, I^F](\vec{x}) \circ U \ .
 \end{aligned} \tag{13}$$

5.2 Two-step registration

Multi-step registration is common practice, often using multiple algorithms. For example, ANTs [2] by default performs affine, then deformable registration, and returns the composition of the resulting transforms. Greer et al. [12] propose a general notation for this scheme: the TwoStep operator, which takes as input two registration algorithms, and yields a composite algorithm as follows:

$$\text{TwoStep}\{\Phi, \Psi\}[I^M, I^F] = \Phi[I^M, I^F] \circ \Psi[I^M \circ \Phi[I^M, I^F], I^F] \ . \tag{14}$$

We show that if Φ is $[W, U]$ equivariant and Ψ is $[U, U]$ equivariant for U and W from a class of transforms \mathcal{T} , then $\text{TwoStep}\{\Phi, \Psi\}$ is $[W, U]$ equivariant. In particular,

$$\begin{aligned}
 &\text{TwoStep}\{\Phi, \Psi\}[I^M \circ W, I^F \circ U] \\
 &= \Phi[I^M \circ W, I^F \circ U] \circ \Psi[I^M \circ W \circ \Phi[I^M \circ W, I^F \circ U], I^F \circ U] \\
 &= W^{-1} \circ \Phi[I^M, I^F] \circ U \circ \Psi[I^M \circ \Phi[I^M, I^F] \circ U, I^F \circ U] \\
 &= W^{-1} \circ \Phi[I^M, I^F] \circ \Psi[I^M \circ \Phi[I^M, I^F], I^F] \circ U \\
 &= W^{-1} \circ \text{TwoStep}\{\Phi, \Psi\}[I^M, I^F] \circ U \ .
 \end{aligned} \tag{15}$$

Therefore, $\text{TwoStep}\{\Phi, \Psi\}$ is $[W, U]$ equivariant. This construction can be applied recursively for an N -step $[W, U]$ equivariant network, and can be combined with the downsampling operator (abbr. as Down) from [39] (see Appendix, B) to make the early stages operate at coarse resolution.

6 Experiments

Architecture. We propose the architecture *Coordinate Attention with Refinement Layers* (CARL),

$$\text{CARL} := \text{TwoStep}\{\text{Down}\{\text{TwoStep}\{\text{Down}\{\Xi_\theta\}\}, \Psi_1\}\}, \Psi_2\} \tag{16}$$

where Ξ_θ is a $[W, U]$ equivariant neural network composed of a translation-equivariant feature encoder and a coordinate attention layer as proposed, and Ψ_i are refinement layers: convolutional

¹At least, for translations of integer multiples of the least common multiple of all convolution strides, and considering the input and output of the convolution to be functions.

networks predicting displacement with architecture and feature counts from [12, 39], and so are $[U, U]$ equivariant. *The overall network is then $[W, U]$ equivariant with respect to translation.*

Losses. In all experiments, we train with LNCC image similarity (LNCC=1-local normalized cross correlation). For regularization, we train initially with a diffusion loss for 1,500 steps, i.e.,

$$\begin{aligned} \mathcal{L} = \text{LNCC}(I^M \circ \text{CARL}[I^M, I^F], I^F) + \text{LNCC}(I^F \circ \text{CARL}[I^F, I^M], I^M) \\ + \lambda \|\nabla(\text{CARL}[I^M, I^F]) - \mathbf{I}\|_F^2 \end{aligned} \quad (17)$$

and then continue training with the GradICON [39] regularizer for 50,000 steps, i.e.,

$$\begin{aligned} \mathcal{L} = \text{LNCC}(I^M \circ \text{CARL}[I^M, I^F], I^F) + \text{LNCC}(I^F \circ \text{CARL}[I^F, I^M], I^M) \\ + \lambda \|\nabla(\text{CARL}[I^M, I^F] \circ \text{CARL}[I^F, I^M]) - \mathbf{I}\|_F^2, \end{aligned} \quad (18)$$

where \mathbf{I} is the identity matrix, and $\lambda > 0$. We use regularization parameter $\lambda = 1.5$ and an Adam optimizer with a learning rate of 0.0001. We remark that diffusion regularization is needed in early steps of training for stability, but GradICON delivers superior final regularity and correspondence by strongly forcing the network towards invertibility while still allowing large deformations.

Instance Optimization (IO). Following GradICON [39], we evaluate with and without 50 steps of Instance Optimization, i.e., since our method does not use human annotations at train time, at deployment we can further optimize (18) on instances of test data to improve performance.

6.1 Deformed retina images

We first demonstrate the importance of several details of our implementation on a dataset consisting of synthetically warped retina segmentations from [39]. In particular, for this experiment, we train three network variants:

- 1) TwoStep{Down{TwoStep{Down{\Psi_0}, \Psi_1}}, \Psi_2}, a multi-step network with each step predicting a displacement field. This is the 1st stage architecture proposed in GradICON [39]. We expect this network to *not* be $[W, U]$ equivariant w.r.t. translation.
- 2) Down{Down{\Xi_\theta}}, a single-step coordinate attention network. We expect this network to be $[W, U]$ equivariant w.r.t translation, but less powerful than 1).
- 3) CARL, Eq. (16). We expect this network to be powerful and $[W, U]$ equivariant to translation.

Each is assessed *without* instance optimization. To assess differences between these network types, we create three variants of the retina dataset:

- 1) **Baseline.** The train set is constructed by warping 14 segmentations from the DRIVE dataset [37], and the test set is constructed by warping the remaining 6 segmentations, with elastic warp parameters as suggested in [39].
- 2) **Shift.** The same as Baseline, but with fixed images shifted by 200 pixels.
- 3) **Scale Shift.** The same as Shift, but with fixed images also scaled to 80% size (See Fig. 3).

Results for this experiment are shown in Fig. 3. We see that when training/testing on the **Baseline** dataset, as expected, all three networks have adequate performance, although the importance of the refinement layers is highlighted when Down{Down{\Xi_\theta}} falls meaningfully behind. When trained and tested on the **Shift** variant, the equivariant networks succeed, while the displacement predicting network fails. Additionally, we see that the equivariant networks *generalize* to the **Shift** test dataset when trained only on **Baseline**. Finally, we see that the equivariant networks also learn on, *and generalize to*, the **Scale Shift** dataset. This result illustrates an important point that we did not prove but observe empirically: while Ξ_θ is formally only $[W, U]$ equivariant to integer translations, in practice it is $[W, U]$ equivariant to deformations that are locally approximately translations, such as scaling. We do see a large variance **between training runs** when training CARL on the **Shift** and **Scale Shift** datasets. That is, specifically when training on Shift or Scale Shift, most trained CARL networks have high performance across all test examples, but for a small fraction of training runs, performance is poor across the whole test set.

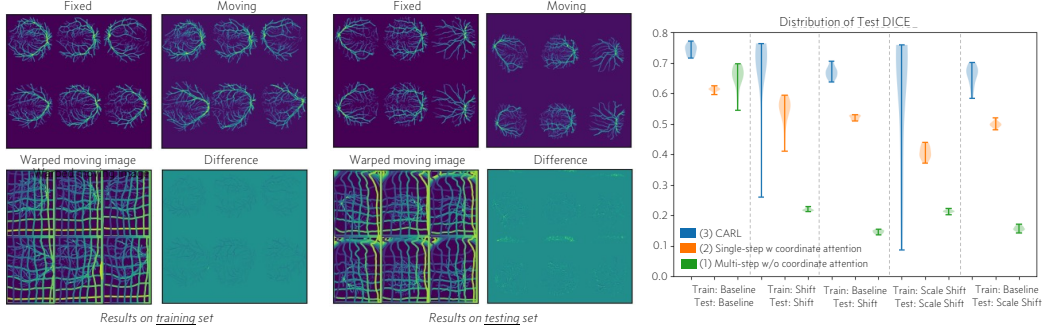


Figure 3: Equivariance allows CARL to generalize out-of-distribution. The *left* figure shows performance CARL on a test set with the same distribution as the training set, where images are *aligned* in scale and translation. The *middle* figure shows generalization to a test set **Scale Shift** where images are *misaligned* in scale and translation. The *right* figure shows the distribution of mean dice performance on the test set, over multiple training runs.

6.2 Performance comparison to other methods

We compare our method to existing approaches from the literature on three datasets. First, we evaluate on the 10 DirLab COPDGene test cases as this is a popular and difficult registration benchmark that allows us to compare our performance to diverse and highly optimized methods. Second, we evaluate on the HCP brain dataset, which allows us to directly compare to two existing equivariant registration methods, EasyReg and KeyMorph. Third, we evaluate on a novel registration task: registering images from the Abdomen1k dataset without registration-specific preprocessing. This dataset has very large translational differences and different fields of view, which causes other unsupervised registration approaches to converge poorly. Our strong equivariance makes this task possible with the LNCC + regularization loss. We aim to present a picture of how our approach will work when applied as specified to new datasets. To this end, *we use the same hyperparameters for all three datasets.*

Lung registration. In order to evaluate our method against the current state of the art for general registration, we use the DirLab lung registration task, which is well standardized and has gained considerable attention in the community. In particular, we train on 999 pairs of images from the COPDGene dataset, and evaluate based on landmark distance in the 10 standard DirLab cases. We follow the data preparation and augmentation suggested in GradICON [39]. Results are listed in Table 1, showing the commonly-used mTRE score as well as the percentage of negative values for the Jacobian determinant ($\%|J|_{<0}$), indicative of the number of folds.

Brain Registration. The existing equivariant image registration methods that we compare to are presented as brain registration methods. We compare to them on the Human Connectome Project (HCP) dataset [43, 33, 34]. We perform evaluation and preprocessing as in [13]. We find that our approach is state of the art in performance. We also artificially translate one image by varying amounts and re-evaluate performance, verifying that GradICON sharply drops in performance under this shift, while our approach and EasyReg are unaffected (see Fig. 4).

Abdomen registration. Abdominal CT-CT datasets can capture the diversity of fields of view of the abdominal CT scan in clinical practice, and the Abdomen1k [27] dataset is curated specifically to do so. Since our method is robust to these differences of field of view because it is $[W, U]$ equivariant to translation, we showcase its performance for inter-subject registration of the Abdomen1K [27] dataset. We train on the first 800 cases of the Abdomen1K dataset, validate on cases 900-1000, and test on cases 800-900. We opt for a minimalist preprocessing: we resample all images to [175, 175, 175] and then divide by the maximum intensity. We test by randomly sampling 30 image pairs and then computing the mean Dice score over manual annotations of the liver, kidney, pancreas, and spleen. We report (Appendix, I) the exact pairs to allow future works to compare to our result. The most important comparison is to GradICON, as our final network, similarity and regularity loss are identical to GradICON’s except that we omit the second 50,000 iteration training step, and replace the first U-Net based Ψ with our custom Ξ_θ . This change produces a dramatic improvement in non-instance-optimization registration accuracy and an improvement in instance-optimized registration accuracy. Results are listed in Table 1. We also check whether the model trained on the Abdomen1k dataset generalizes to the Learn2Reg Abdomen CT-CT challenge set. Performance is better than

other unsupervised approaches including the keypoint-based SAME++, but does not match the best supervised methods trained using the Learn2Reg CT-CT training set *and segmentations*.

Table 1: Performance comparison on Abdomen 1K, HCP, DirLab, and Learn2Reg Abdomen CTCT dataset. Methods using segmentation maps are denoted with *.

Method	DICE↑	$\% J _{<0} \downarrow$	Method	mTRE↓	$\% J _{<0} \downarrow$	Method	DICE↑
Abdomen1K			DirLab			L2R Abd. CTCT Test set	
ANTs [2]	45.4	0	ANTs [2]	1.79	0	ConvexAdam [36]*	69
VoxelMorph [3]	59.3	-	Elastix [25]	1.32	-	LapIRN [29]*	67
GradICON [39]	49.6	7e-1	VoxelMorph [3]	9.88	0	Estienne [10]*	69
GradICON(IO) [39]	71.0	4e-2	LapIRN [29]	2.92	0	corrField [15, 18]	49
ConstrICON [13]	65.2	7e-4	RRN [16]	0.83	-	PIMed [20]	49
ConstrICON(IO) [13]	66.8	2e-3	Hering et al [19]	2.00	6e-2	PDD-Net [17]	49
CARL	74.1	3e-1	GraphRegNet [15]	1.34	-	Joutard [20]	40
CARL(IO)	75.9	4e-3	PLOSL [46]	3.84	0	NiftyReg [28]	45
HCP			PLOSL(IO) [46]	1.53	0	Cunnarsson [14]	43
ANTs [2]	77.2	0	PTVReg [44]	0.83	-	L2R Abd. CTCT Val. set	
uniGradICON [38]	76.2	6e-5	GradICON [39]	1.93	3e-4	SAME++(IO) [40]	49
uniGradICON(IO) [38]	78.9	2e-4	GradICON [39]	1.31	2e-4	UniGradICON(IO) [38]	52
GradICON [13]	78.6	1e-3	ConstrICON [13]	2.03	7e-6	CARL(IO)	53
GradICON(IO) [13]	80.2	5e-4	ConstrICON(IO) [13]	1.62	3e-6		
ConstrICON [13]	79.3	4e-6	uniGradICON [38]	2.26	9e-5		
ConstrICON(IO) [13]	80.1	0	uniGradICON(IO) [38]	1.40	9e-5		
Easyreg [22]	78.8	-	CARL	2.58	2e-6		
KeyMorph [48]	67.2	0	CARL(IO)	1.52	3e-6		
CARL	78.8	5e-4					
CARL(IO)	80.4	3e-4					

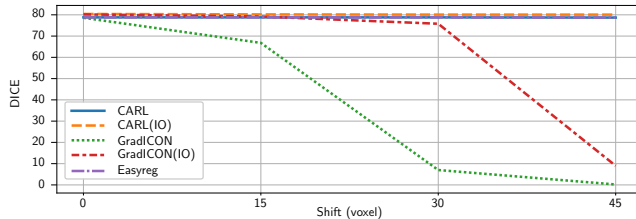


Figure 4: HCP evaluation while translating one image. CARL and EasyReg are unaffected by translation due to $[W, U]$ equivariance. GradICON DICE drops significantly for large translations due to its $[U, U]$ equivariance.

6.3 Limitations

Notably absent from our results are equivariance to rotations. This does not doom CARL, as our driving goal was to accurately register abdominal organs, where the rough rotation is known from the image metadata, and the driving issue is discrepancy in translation. For other areas of application, such as fetal MRI registration as tackled by E-CNN [6], translation equivariance is much less important since moments-based initialization works well, and rotational equivariance takes foremost importance as the rough orientation of the fetus with respect to the scanner is initially unknown. Our derivation of $[W, U]$ equivariance to translation (Sec. 5) holds for $[W, U]$ equivariance with respect to rotation if Conv_θ is replaced with a rotation equivariant encoder such as [23] or [30], but unlike for translation equivariant encoders, the assumption that attention maps should have small spatial support after training does not hold following any training procedure of a Ξ_θ with rotationally equivariant encoders that we have attempted; a dedicated loss to encourage small spatial support may be required.

Our method is expensive to evaluate: registering a pair of images with a forward pass takes 8 seconds, and instance optimization takes 850 seconds on a NVIDIA RTX 6000 GPU. However, we consider this a minor issue at the moment, and focus on accuracy, as we anticipate that hardware and software for rapidly computing the flash attention kernel will rapidly improve in the near future.

7 Conclusion

We demonstrated that our proposed multi-step architecture has a novel combination of strong equivariance and precise handling of complex and high resolution deformations. We show that it has close to state of the art accuracy on lung registration when compared to a competitive leaderboard, excellent performance on brain registration with empirically verified equivariance to translations, and is capable of registering raw abdomen scans with differing fields of view which were not amenable to existing unsupervised registration approaches.

Acknowledgments and Disclosure of Funding

The research reported in this publication was supported by the National Institutes of Health (NIH) under award numbers NIH 1 R01 HL149877, NIH 1 R01 EB028283, NIH 1 R01 AR082684, 1 R21 MH132982, and NIH RF1 MH126732. The content is solely the responsibility of the authors and does not necessarily represent the official views of the NIH.

References

- [1] Abhari, J., Ashok, A.: Mitigating racial biases for machine learning based skin cancer detection. In: Proceedings of the Twenty-Fourth International Symposium on Theory, Algorithmic Foundations, and Protocol Design for Mobile Networks and Mobile Computing. p. 556–561. MobiHoc '23, Association for Computing Machinery, New York, NY, USA (2023)
- [2] Avants, B.B., Epstein, C.L., Grossman, M., Gee, J.C.: Symmetric diffeomorphic image registration with cross-correlation: evaluating automated labeling of elderly and neurodegenerative brain. *MedIA* **12**(1), 26–41 (2008)
- [3] Balakrishnan, G., Zhao, A., Sabuncu, M.R., Guttag, J., Dalca, A.V.: VoxelMorph: a learning framework for deformable medical image registration. *TMI* **38**(8), 1788–1800 (2019)
- [4] Bay, H., Tuytelaars, T., Van Gool, L.: SURF: Speeded up robust features. In: Leonardis, A., Bischof, H., Pinz, A. (eds.) ECCV (2006)
- [5] Billot, B., Greve, D.N., Puonti, O., Thielscher, A., Van Leemput, K., Fischl, B., Dalca, A.V., Iglesias, J.E.: SynthSeg: Segmentation of brain MRI scans of any contrast and resolution without retraining. *MedIA* **86**, 102789 (2023)
- [6] Billot, B., Moyer, D., Karani, N., Hoffmann, M., Turk, E.A., Grant, E., Golland, P.: Equivariant and denoising CNNs to decouple intensity and spatial features for motion tracking in fetal brain MRI. In: MIDL (2023)
- [7] Cohen, T., Welling, M.: Group equivariant convolutional networks. In: ICML. pp. 2990–2999. PMLR (2016)
- [8] Dalca, A.V., Balakrishnan, G., Guttag, J., Sabuncu, M.R.: Unsupervised learning for fast probabilistic diffeomorphic registration. In: MICCAI (2018)
- [9] Dao, T., Fu, D., Ermon, S., Rudra, A., Ré, C.: Flashattention: Fast and memory-efficient exact attention with io-awareness. *NeurIPS* (2022)
- [10] Estienne, T., Vakalopoulou, M., Battistella, E., Carré, A., Henry, T., Lerousseau, M., Robert, C., Paragios, N., Deutsch, E.: Deep learning based registration using spatial gradients and noisy segmentation labels. In: Segmentation, Classification, and Registration of Multi-modality Medical Imaging Data: MICCAI 2020 Challenges. pp. 87–93. Springer (2021)
- [11] Fukushima, K.: Neocognitron: A self-organizing neural network model for a mechanism of pattern recognition unaffected by shift in position. *Biological Cybernetics* **36**, 193–202 (1980)
- [12] Greer, H., Kwitt, R., Vialard, F.X., Niethammer, M.: ICON: Learning regular maps through inverse consistency. In: ICCV (2021)
- [13] Greer, H., Tian, L., Vialard, F.X., Kwitt, R., Bouix, S., San Jose Estepar, R., Rushmore, R., Niethammer, M.: Inverse consistency by construction for multistep deep registration. In: MICCAI. pp. 688–698. Springer (2023)
- [14] Gunnarsson, N., Sjölund, J., Schön, T.B.: Learning a deformable registration pyramid. In: MICCAI. pp. 80–86. Springer (2020)
- [15] Hansen, L., Heinrich, M.P.: GraphRegNet: Deep graph regularisation networks on sparse keypoints for dense registration of 3D lung CTs. *TMI* **40**(9), 2246–2257 (2021)

- [16] He, X., Guo, J., Zhang, X., Bi, H., Gerard, S., Kaczka, D., Motahari, A., Hoffman, E., Reinhardt, J., Barr, R.G., Angelini, E., Laine, A.: Recursive refinement network for deformable lung registration between exhale and inhale CT scans. arXiv preprint arXiv:2106.07608 (2021)
- [17] Heinrich, M.P.: Closing the gap between deep and conventional image registration using probabilistic dense displacement networks. In: MICCAI. pp. 50–58. Springer (2019)
- [18] Heinrich, M.P., Handels, H., Simpson, I.J.: Estimating large lung motion in copd patients by symmetric regularised correspondence fields. In: MICCAI. pp. 338–345. Springer (2015)
- [19] Hering, A., Häger, S., Moltz, J., Lessmann, N., Heldmann, S., van Ginneken, B.: CNN-based lung CT registration with multiple anatomical constraints. *MedIA* **72**, 102139 (2021)
- [20] Hering, A., Hansen, L., Mok, T.C., Chung, A.C., Siebert, H., Häger, S., Lange, A., Kuckertz, S., Heldmann, S., Shao, W., et al.: Learn2reg: comprehensive multi-task medical image registration challenge, dataset and evaluation in the era of deep learning. *TMI* **42**(3), 697–712 (2022)
- [21] Honkamaa, J., Marttinen, P.: Asymreg: Robust symmetric image registration using anti-symmetric formulation and deformation inversion layers. arXiv preprint arXiv:2303.10211 (2023)
- [22] Iglesias, J.E.: A ready-to-use machine learning tool for symmetric multi-modality registration of brain mri. *Scientific Reports* **13**(1), 6657 (2023)
- [23] Karras, T., Aittala, M., Laine, S., Härkönen, E., Hellsten, J., Lehtinen, J., Aila, T.: Alias-free generative adversarial networks. *NeurIPS* **34**, 852–863 (2021)
- [24] Kleesiek, J., Urban, G., Hubert, A., Schwarz, D., Maier-Hein, K., Bendszus, M., Biller, A.: Deep mri brain extraction: A 3d convolutional neural network for skull stripping. *NeuroImage* **129**, 460–469 (2016)
- [25] Klein, S., Staring, M., Murphy, K., Viergever, M.A., Pluim, J.P.: Elastix: a toolbox for intensity-based medical image registration. *TMI* **29**(1), 196–205 (2009)
- [26] Lowe, D.G.: Distinctive image features from scale-invariant keypoints. *IJCV* **60**, 91–110 (2004)
- [27] Ma, J., Zhang, Y., Gu, S., Zhu, C., Ge, C., Zhang, Y., An, X., Wang, C., Wang, Q., Liu, X., Cao, S., Zhang, Q., Liu, S., Wang, Y., Li, Y., He, J., Yang, X.: Abdoment-1k: Is abdominal organ segmentation a solved problem? *TPAMI* **44**(10), 6695–6714 (2022)
- [28] Modat, M., Ridgway, G.R., Taylor, Z.A., Lehmann, M., Barnes, J., Hawkes, D.J., Fox, N.C., Ourselin, S.: Fast free-form deformation using graphics processing units. *Comput. Methods Programs Biomed.* **98**(3), 278–284 (2010)
- [29] Mok, T.C., Chung, A.: Large deformation diffeomorphic image registration with Laplacian pyramid networks. In: MICCAI (2020)
- [30] Moyer, D., Abaci Turk, E., Grant, P.E., Wells, W.M., Golland, P.: Equivariant filters for efficient tracking in 3d imaging. In: MICCAI. pp. 193–202. Springer (2021)
- [31] Nordling, L., Öfverstedt, J., Lindblad, J., Sladoje, N.: Contrastive learning of equivariant image representations for multimodal deformable registration. *ISBI* pp. 1–5 (2023)
- [32] Parikh, A., Täckström, O., Das, D., Uszkoreit, J.: A decomposable attention model for natural language inference. In: Su, J., Duh, K., Carreras, X. (eds.) *EMNLP*. pp. 2249–2255 (Nov 2016)
- [33] Rushmore, R.J., Sutherland, K., Carrington, H., Chen, J., Halle, M., Lasso, A., Papadimitriou, G., Prunier, N., Rizzoni, E., Vessey, B., Wilson-Braun, P., Rathi, Y., Kubicki, M., Bouix, S., Yeterian, E., Makris, N.: Anatomically curated segmentation of human subcortical structures in high resolution magnetic resonance imaging: An open science approach. *Front. Neuroanat.* **16** (2022)
- [34] Rushmore, R.J., Sutherland, K., Carrington, H., Chen, J., Halle, M., Lasso, A., Papadimitriou, G., Prunier, N., Rizzoni, E., Vessey, B., Wilson-Braun, P., Rathi, Y., Kubicki, M., Bouix, S., Yeterian, E., Makris, N.: HOA-2/SubcorticalParcellations: release-50-subjects-1.1.0 (sep 2022)

- [35] Shen, Z., Han, X., Xu, Z., Niethammer, M.: Networks for joint affine and non-parametric image registration. In: CVPR (2019)
- [36] Siebert, H., Hansen, L., Heinrich, M.P.: Fast 3d registration with accurate optimisation and little learning for learn2reg 2021. In: MICCAI. pp. 174–179. Springer (2021)
- [37] Staal, J., Abràmoff, M.D., Niemeijer, M., Viergever, M.A., Van Ginneken, B.: Ridge-based vessel segmentation in color images of the retina. TMI **23**(4), 501–509 (2004)
- [38] Tian, L., Greer, H., Kwitt, R., Vialard, F.X., Estepar, R.S.J., Bouix, S., Rushmore, R., Niethammer, M.: uniGradICON: A foundation model for medical image registration. arXiv preprint arXiv:2403.05780 (2024)
- [39] Tian, L., Greer, H., Vialard, F.X., Kwitt, R., Estépar, R.S.J., Niethammer, M.: GradICON: Approximate diffeomorphisms via gradient inverse consistency. CVPR pp. 18084–18094 (2022)
- [40] Tian, L., Li, Z., Liu, F., Bai, X., Ge, J., Lu, L., Niethammer, M., Ye, X., Yan, K., Jin, D.: SAME++: A self-supervised anatomical embeddings enhanced medical image registration framework using stable sampling and regularized transformation. arXiv preprint arXiv:2311.14986 (2023)
- [41] Toga, A.W., Thompson, P.M.: The role of image registration in brain mapping. Image and vision computing **19**(1-2), 3–24 (2001)
- [42] Truong, P., Danelljan, M., Yu, F., Van Gool, L.: Warp consistency for unsupervised learning of dense correspondences. In: ICCV (2021)
- [43] Van Essen, D.C., Ugurbil, K., Auerbach, E., Barch, D., Behrens, T.E., Bucholz, R., Chang, A., Chen, L., Corbetta, M., Curtiss, S.W., Della Penna, S., Feinberg, D., Glasser, M.F., Harel, N., Heath, A.C., Larson-Prior, L., Marcus, D., Michalareas, G., Moeller, S., Oostenfeld, R., Peterson, S.E., Prior, F., Schlaggar, B.L., Smith, S.M., Snyder, A.Z., Xu, J., Yacoub, E., Consortium, W.M.H.: The human connectome project: a data acquisition perspective. NeuroImage **62**(4), 2222–2231 (2012)
- [44] Vishnevskiy, V., Gass, T., Székely, G., Tanner, C., Goksel, O.: Isotropic total variation regularization of displacements in parametric image registration. TMI **36**(2), 385–395 (2017)
- [45] Wang, A.Q., Yu, E.M., Dalca, A.V., Sabuncu, M.R.: A robust and interpretable deep learning framework for multi-modal registration via keypoints. MedIA **90**, 102962 (2023)
- [46] Wang, D., Pan, Y., Durumeric, O.C., Reinhardt, J.M., Hoffman, E.A., Schroeder, J.D., Christensen, G.E.: PLOSL: Population learning followed by one shot learning pulmonary image registration using tissue volume preserving and vesselness constraints. MedIA **79**, 102434 (2022)
- [47] Yang, X., Kwitt, R., Styner, M., Niethammer, M.: Quicksilver: Fast predictive image registration—a deep learning approach. NeuroImage **158**, 378–396 (2017)
- [48] Yu, E.M., Wang, A.Q., Dalca, A.V., Sabuncu, M.R.: KeyMorph: Robust multi-modal affine registration via unsupervised keypoint detection. In: MIDL (2022)

Supplemental Material

A Per Structure DICE Box Plot

To provide a more comprehensive picture of how different registration algorithms perform for different brain structures or organs (instead of purely reporting averages) Figs. 5 and 6 show anatomy-specific boxplots. We observe especially strong performance for CARL on the Abdomen1k dataset (Fig. 6) with excellent registration results for liver, kidney, and spleen.

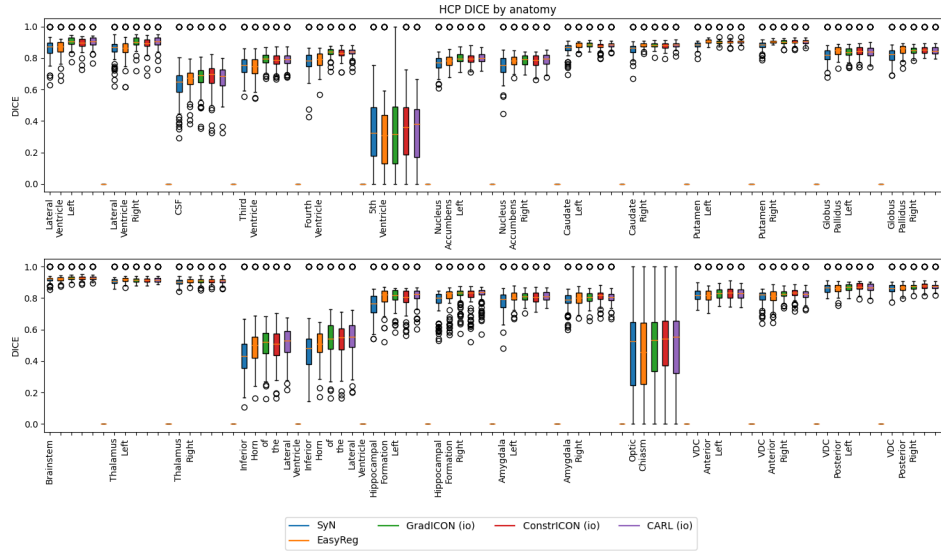


Figure 5: Per structure DICE scores on the HCP dataset

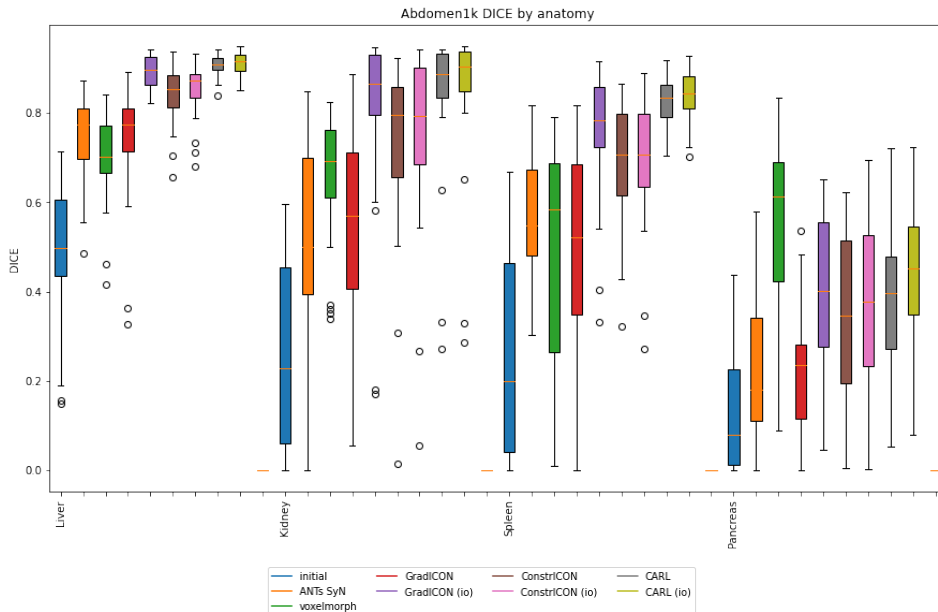


Figure 6: Per structure DICE scores on the Abdomen1k dataset

B Resolution, Downsampling, and Coordinates

We use an internal convention that regardless of resolution, images have coordinates ranging from $(0, 0, 0)$ to $(1, 1, 1)$. Thus, a transform, a function from $[0, 1]^D \rightarrow \mathcal{R}^N$, can be applied to an image of any resolution. This allows us to construct a multiresolution, multi-step registration algorithm using TwoStep and the operator Downsample defined in [12] as

$$\text{Downsample}\{\Phi\}[I^M, I^F] = \Phi[\text{averagePool}(I^M, 2), \text{averagePool}(I^F, 2)]. \quad (19)$$

C Implementing the diffeomorphism-to-diffeomorphism case

We can use coordinate attention to solve the diffeomorphism-to-diffeomorphism registration problem with a neural network $\Xi_{\mathcal{F}}$ (shown in the left part of Fig. 7).

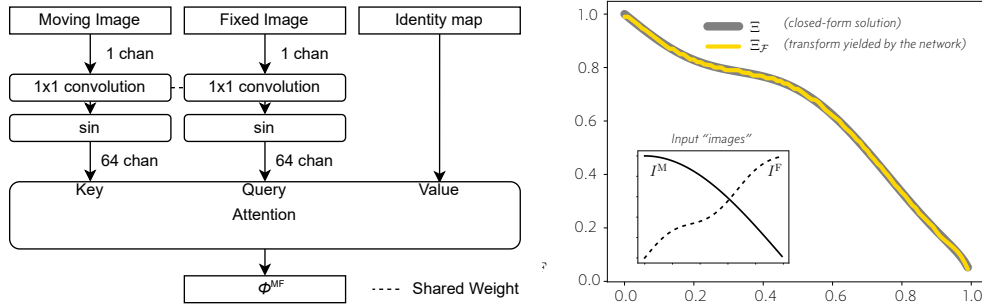


Figure 7: Left: Neural network $\Xi_{\mathcal{F}}$ implementing Ξ . Right: Result of registering the 1-dimensional "images" $I^M : [0, 1] \rightarrow [0, 1], x \mapsto \cos(\frac{\pi}{2}x)$ and $I^F : [0, 1] \rightarrow [0, 1], x \mapsto x + 0.07 \sin(3\pi x)$ via Ξ and $\Xi_{\mathcal{F}}$, illustrating that the resulting maps are equivalent. Ξ is computable here as these images are invertible and smooth. The neural network output (gold) closely matches the analytical solution (i.e., $\Xi[I^M, I^F] = I^{M^{-1}} \circ I^F = \frac{2}{\pi} \cos^{-1}(x + 0.07 \sin(3\pi x))$), gray. Best-viewed in color.

The input functions I^M, I^F , and the output transform are approximated as arrays of voxels. The functional Ξ such that $\Xi[I^M, I^F] := (I^M)^{-1} \circ I^F$ (which only operates on images that are diffeomorphic) can be directly implemented, without training, using standard neural network components. We refer to this implementation as $\Xi_{\mathcal{F}}$. The intention is to map each voxel in the moving image into a high dimensional vector that will have a large dot product with the corresponding voxel in the fixed image with the same value, and then compute the attention matrix with the embedded fixed image voxels as the queries and the embedded moving image voxels as the keys. Subsequently, we can compute the center of mass of the attention masks (i.e., where each fixed image voxel matches on the moving image) by setting the values to be the raw coordinates of the moving image voxels. We choose for the embedding a 1×1 convolution with large weights followed by a sine-nonlinearity, which has the desired property of two vectors having a large dot product only when their input intensities are similar. Because our images are diffeomorphisms, we know a-priori that the input intensity of our moving image will only be close to intensities of the fixed image in a small region. We verify that this network, without any training, reproduces Ξ when applied to input images that are diffeomorphisms, see Fig. 7 (right).

C.1 Limitation on equivariance feasibility

In Sec. C, we turned images into features using 1×1 convolution followed by a sine nonlinearity which, since it is a function applied pointwise, is perfectly equivariant. This worked since the images to be registered were diffeomorphisms, and hence each intensity vector was unique. However, since, as we are about to prove, we cannot achieve equivariance to arbitrary diffeomorphisms for registering real images, we have to sacrifice some equivariance in order to expand the set of valid inputs. This drives our choice to target translation equivariance.

Claim. It is impossible to have an algorithm that is $[W, U]$ equivariant to arbitrary smooth deformations and can be applied to arbitrary images.

Counterexample. Assume that Ψ is a $[W, U]$ equivariant algorithm for all $W, U \in$ diffeomorphisms, and that is valid for all input images. We ask it to register the images $I^A, I^B := 0$. Then, for any W , $I^M \circ W = I^M$ so we need $\Psi[0, 0] = W^{-1} \circ \Psi[0, 0]$, or $id = W^{-1}$. This yields a contradiction.

We conclude that an algorithm must either only apply to a subset of possible images, or only be $[W, U]$ equivariant to a subset of all diffeomorphisms. If there is a valid input image I and a nonzero transform T such that $I \circ T = I$, then T cannot be in the class of transforms with respect to which Φ is $[W, U]$ equivariant. For a simple example, an algorithm that registers images of perfect circles cannot be $[W, U]$ equivariant to rotations. For a practical example, since brain-extracted brain images have large areas outside the brain that are exactly zero, algorithms that register such preprocessed brain images cannot be $[W, U]$ equivariant to transforms that are identity everywhere in the brain but have deformations outside the brain. To modify $\Xi_{\mathcal{F}}$ so that it can apply to a broader class of images other than "images that happen to be diffeomorphisms", we thus have to restrict the transforms with respect to which it is $[W, U]$ equivariant. This drives our choice to use translation equivariant encoders, and is likely connected to why we have so far been unable to train coordinate attention with a rotation equivariant encoder.

C.2 Guarantee given equivariance

While it is unfortunate that we cannot achieve $[W, U]$ equivariance to arbitrary diffeomorphisms for arbitrary input images, there is great advantage to expanding \mathcal{T} . For any input image pair where the images can be made to match exactly for a transform in \mathcal{T} , an algorithm that is Inverse Consistent and $[W, U]$ equivariant with respect to \mathcal{T} will output that transform. We see this as follows.

Assume Φ is inverse consistent and $[W, U]$ equivariant with respect to \mathcal{T} , and $I^M \circ U = I^F$ for a $U \in \mathcal{T}$. Then

$$\Phi[I^M, I^F] \tag{20}$$

$$= \Phi[I^M, I^M \circ U] \tag{21}$$

$$= \Phi[I^M, I^M \circ U] \tag{22}$$

$$= U, \tag{23}$$

where $\Phi[I^M, I^M \circ U] = \Phi[I^M, I^M \circ U]$ holds because of the $[W, U]$ equivariance with W being the identity transform.

D Comparison to KeyMorph on IXI brain.

A strong competitor to our method is KeyMorph [45]. In Sec 6.2 we compared to a version of their model we trained ourselves using the published KeyMorph code. To verify our relative performance, we also train our model on the IXI dataset using the KeyMorph splits, preprocessing and evaluation, and compare to the published KeyMorph pretrained weights. We compare on unimodal registration. Tab. 2 shows that CARL outperforms KeyMorph and ANTs.

Note that KeyMorph evaluates using DICE on segmentations produced by SynthSeg [5]- this precludes direct comparison to EasyReg, which uses SynthSeg in its forward pass. With this caveat in mind, by this metric EasyReg has a DICE 82.4.

Table 2: Results on IXI. CARL performs well compared to KeyMorph. Following KeyMorph’s protocol we evaluate using segmentations produced with SynthSeg [5], and perform brain extraction using a different U-Net based on [24].

Method	DICE
KeyMorph [45]	68.5
ANTs SyN [2]	67.1
CARL	75.5
CARL (IO)	77.5

E Performance implications of two step registration

We observed in Sec. 6.1 that Ξ_θ trains significantly better as the beginning of a multistep algorithm than on its own. Here, we examine why that may be, while removing as much complexity as possible. Our finding suggests that two step registration assists training by functioning as a similarity measure with better capture radius.

First, we briefly pretrain a single step network Φ on the **Baseline** task from Sec. 6.1, i.e. not to convergence. Then, we examine the loss landscape of a trivial "fixedTranslation" neural network τ to register **Baseline**. This network has a single parameter, t , and it ignores its input images and always shifts images to the right by t : that is

$$\tau[I^M, I^F](\vec{r}) = \vec{r} + \begin{bmatrix} t \\ 0 \end{bmatrix}. \quad (24)$$

The optimal value of t is zero since there is no bias towards left or right shift of images in this dataset- but if we were to train τ on LNCC similarity, how well would the gradients drive t to zero?

We plot $LNCC(I^M \circ \tau[I^M, I^F], I^F)$ against t compared to $LNCC(I^M \circ TwoStep\{\tau, \Phi\}[I^M, I^F], I^F)$. We also plot $\frac{\partial}{\partial t} LNCC(I^M \circ \tau[I^M, I^F], I^F)$ and $\frac{\partial}{\partial t} LNCC(I^M \circ TwoStep\{\tau, \Phi\}[I^M, I^F], I^F)$ using pytorch's back-propagation. Fig. 8 shows the result indicating that multi-step registration results in better capture radius.

Effectively, when two step network $TwoStep\{\tau, \Phi\}$ is trained with an LNCC loss, the loss function seen by τ is not simply LNCC, but instead the performance of Φ , which is an implicit loss function with a better capture radius.

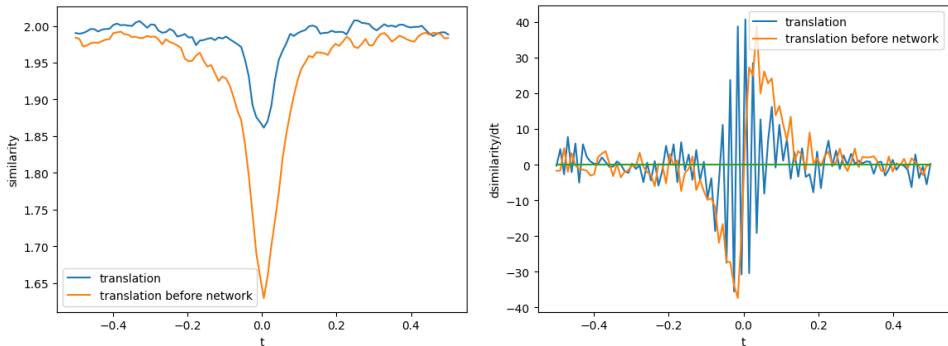


Figure 8: The loss of $TwoStep\{\tau, \Phi\}$ (i.e., translation before network) as a function of t is much better behaved than the loss of τ (i.e., translation) as a function of t . The capture radius of the former is larger and the loss is overall smoother close to the correct solution as shown on the right.

F Computational Budget

Each 50,000 step training run of CARL takes 7 days on 4 RTX A6000 GPUs. In total, 264 GPU days were spent developing the CARL architecture and training the final models.

An additional 45 GPU days were spent training comparison methods. 14 server days were spent training KeyMorph variants, although the published KeyMorph code is io-bound and did not significantly load the server's GPU.

G Comparison Methods Details

G.1 Abdomen1k

For Abdomen1k, we trained all methods using their published code and default hyperparameters.

G.2 DirLab Lung

On the DirLab challenge set, all results of comparison methods are taken from the literature. Results of ANTs, Elastix, Voxelmorph, and LapIRN are from [39]. The remainder are from their associated publications.

G.3 HCP

On HCP, we evaluated ANTs using code from [39]. Results of GradICON, and ConstrICON are from the ConstrICON publication. We evaluated KeyMorph by training a model on the HCP Dataset using KeyMorph’s published code and hyperparameters for the IXI dataset. We evaluated Easyreg using its published weights, which are advertised to be appropriate for the HCP dataset. We measured the equivariance of the GradICON method using GradICON’s published code and weights.

H Potential Societal Impacts

We seriously consider the potential societal impacts of our work. Potential positive impacts would be mediated through improved medical image registration accuracy. Registration is used in tasks such as cancer treatment planning, population studies, lung volume and motion measurement, and basic research on brain anatomy. There is a risk that a deep model trained to perform a medical task may underperform on marginalized groups. For example, some studies of melanoma classifiers have found that racially homogeneous training sets lead to disparate health impacts on marginalized groups through misdiagnosis [1]. This could be a subject of future registration equity research, using test datasets that are annotated with demographic information.

I Abdomen Test Pairs

We used the following 30 image pairs to evaluate our abdomen registration experiments.

00817 00872, 00808 00832, 00815 00863, 00857 00860, 00883 00848, 00826 00812, 00862 00803, 00849 00855, 00877 00800, 00857 00834, 00829 00875, 00813 00840, 00803 00802, 00803 00883, 00869 00801, 00848 00887, 00827 00854, 00803 00867, 00828 00856, 00863 00870, 00829 00844, 00829 00886, 00828 00858, 00837 00802, 00853 00871, 00882 00812, 00823 00880, 00837 00815, 00842 00864, 00854 00864